HELSINKI UNIVERSITY OF TECHNOLOGY
TECHNISCHE UNIVERSITÄT HELSINKI
UNIVERSITE DE TECHNOLOGIE D'HELSINKI

Computational results for the superconvergence and postprocessing of MITC plate elements

Jarkko Niiranen, Institute of Mathematics, TKK, Finland

in collaboration with

Mikko Lyly, CSC — Scientific Computing Ltd., Finland

Rolf Stenberg, Institute of Mathematics, TKK, Finland

Outline

Introduction

MITC finite elements for Reissner—Mindlin plates

Superconvergence and postprocessing

Computational results

Conclusions

Introduction

- The original deflection approximation is superconvergent compared to a certain interpolant.
- The postprocessed deflection approximation is a polynomial of one degree higher than the original one.
- It is constructed by utilizing the superconvergence property, which gives accuracy of one degree higher than the original one.
- The postprocessing is local, which implies low computational costs.

MITC finite elements for Reissner—Mindlin plates

- The plate is assumed to be
  - — linearly elastic
  - — isotropic, with
  - — the shear modulus G and
  - — the Poissonin ratio ν.
- The undeformed plate midsurface $\Omega \subset \mathbb{R}^2$ is a convex polygon.
- The plate thickness $t << \text{diam}(\Omega)$ is constant.

Let the boundary conditions on Γ be

— clamped,

— simply supported or

— free.

Then the Reissner—Mindlin plate problem reads:

Problem. *For the loading* $g \in H^{-1}(\Omega)$ *find the deflection* $w \in \{v \in H^1(\Omega) \mid v_{|\Gamma_C} = 0,\ v_{|\Gamma_{SS}} = 0\}$ *and the rotation* $\boldsymbol{\beta} \in \{\boldsymbol{\eta} \in [H^1(\Omega)]^2 \mid \boldsymbol{\eta}_{|\Gamma_C} = \mathbf{0},\ (\boldsymbol{\eta} \cdot \boldsymbol{\tau})_{|\Gamma_{SS}} = 0\}$ *such that*

$$a(\boldsymbol{\beta}, \boldsymbol{\eta}) + \frac{1}{t^2}(\nabla w - \boldsymbol{\beta}, \nabla v - \boldsymbol{\eta}) = (g, v) \ \ \forall (v, \boldsymbol{\eta}) \in W \times \boldsymbol{V},$$

where the bending bilinear form is, with the linear strain $\boldsymbol{\varepsilon}$,

$$a(\boldsymbol{\phi}, \boldsymbol{\eta}) = \frac{1}{6}\{(\boldsymbol{\varepsilon}(\boldsymbol{\phi}), \boldsymbol{\varepsilon}(\boldsymbol{\eta})) + \frac{\nu}{1-\nu}(\operatorname{div} \boldsymbol{\phi}, \operatorname{div} \boldsymbol{\eta})\}.$$

The polynomial interpolation for the MITC finite element method is

- for the deflection approximation $w_h \in W_h$ of order k
- for the components of the rotation approximation $\boldsymbol{\beta}_h \in \boldsymbol{V}_h$

— of order k, enriched by

— the interior bubbles of order $k+1$.

Method. *(Bathe, Brezzi and Fortin 1989) Find* $w_h \in W_h \subset W$ *and* $\boldsymbol{\beta}_h \in \boldsymbol{V}_h \subset \boldsymbol{V}$ *such that*

$$a(\boldsymbol{\beta}_h, \boldsymbol{\eta}) + \frac{1}{t^2}(\boldsymbol{R}_h(\nabla w_h - \boldsymbol{\beta}_h), \boldsymbol{R}_h(\nabla v - \boldsymbol{\eta})) = (g, v) \quad \forall (v, \boldsymbol{\eta}) \in W_h \times \boldsymbol{V}_h,$$

where the reduction operator $\boldsymbol{R}_h$ *maps the shear stress into the rotated Raviart—Thomas polynomial space of order* $k-1$.

Superconvergence and postprocessing

The interpolation operator $I_h : H^s(\Omega) \to W_h$, $s > 1$, is defined through the conditions

$$(v - I_h v)(a) = 0 \;\; \forall \text{ vertices } a \in K,$$
$$\langle v - I_h v, p\rangle_E = 0 \;\; \forall p \in P_{k-2}(E) \;\; \forall \text{ edges } E \subset K,$$
$$(v - I_h v, p)_K = 0 \;\; \forall p \in P_{k-3}(K).$$

The reduction and interpolation operators are closely related:

$$\boldsymbol{R}_h \nabla v = \nabla I_h v \;\; \forall v \in H^s(\Omega), \;\; s \geq 2.$$

Superconvergence

For the deflection approximation w_h of order k,
with the mesh size h, it holds:

$$\|w - w_h\|_1 \leq Ch^k,$$

where the exact deflection w is assumed to be smooth.

For the deflection approximation w_h and the interpolant $I_h w$
it holds:

Theorem 1. *Assuming a smooth solution,*

$$\|I_h w - w_h\|_1 \leq C(h + t)h^k.$$

Postprocessing

- The original deflection approximation is of order k in the element K:

$$w_{h|K} \in P_k(K).$$

- The postprocessed deflection approximation is of order $k+1$ in the element K:

$$w^*_{h|K} \in P_{k+1}(K) = P_k(K) \oplus \widehat{W}(K) \oplus \overline{W}(K).$$

- The new degrees of freedom of order $k+1$, corresponding to the

— element boundaries E, space $\widehat{W}(K)$, and

— element interior, space $\overline{W}(K)$,

are added to the original deflection approximation.

The postprocessing method is based on the definition of the shear stress:

$$\boldsymbol{q} = \frac{1}{t^2}(\nabla w - \boldsymbol{\beta}) \quad \text{or} \quad \nabla w = \boldsymbol{\beta} + t^2 \boldsymbol{q}.$$

Postprocessing scheme. *Find the local postprocessed deflection approximation* $w^*_{h|K} \in P_{k+1}(K)$ *such that*

$$I_h w^*_h = w_h \ \textit{ in the element } K,$$

$$\langle \nabla w^*_h \cdot \boldsymbol{\tau}_E, \nabla \hat{v} \cdot \boldsymbol{\tau}_E \rangle_E = \langle (\boldsymbol{\beta}_h + t^2 \boldsymbol{q}_h) \cdot \boldsymbol{\tau}_E, \nabla \hat{v} \cdot \boldsymbol{\tau}_E \rangle_E \ \ \forall \hat{v} \in \widehat{W}(K),$$

$$(\nabla w^*_h, \nabla \bar{v})_K = (\boldsymbol{\beta}_h + t^2 \boldsymbol{q}_h, \nabla \bar{v})_K \ \ \forall \bar{v} \in \overline{W}(K).$$

In the postprocessing we utilize the superconvergence of the original deflection approximation,

$$\|I_h w - w_h\|_1 \leq C(h+t)h^k.$$

Theorem 2. *For the postprocessed deflection approximation* w_h^* *it holds, assuming a smooth solution,*

$$\|w - w_h^*\|_1 \leq C(h+t)h^k.$$

This is an error estimate of order $h+t$ better than the original one,

$$\|w - w_h\|_1 \leq Ch^k.$$

According to the computational results, a corresponding accuracy improvement holds also in the L^2-norm.

Computational results

- The following semi-infinite plate is considered:
  - — the midsurface $\Omega = \{(x, y) \in \mathbb{R}^2 \mid y > 0\}$
  - — Poisson ratio $\nu = 0.3$
  - — shear modulus $G = \frac{1}{2(1+\nu)}$
  - — thickness $t = 0.01$
  - — loading $g = \frac{1}{G} \cos x$.
- For the boundary $\Gamma = \{(x, y) \in \mathbb{R}^2 \mid y = 0\}$ two different types of boundary conditions are imposed:
  - — simply supported or
  - — free.
- The discretized domain is $\overline{D} = [0, \pi/2] \times [0, 3\pi/2]$.

Accuracy for the uniform meshes — Interior domain

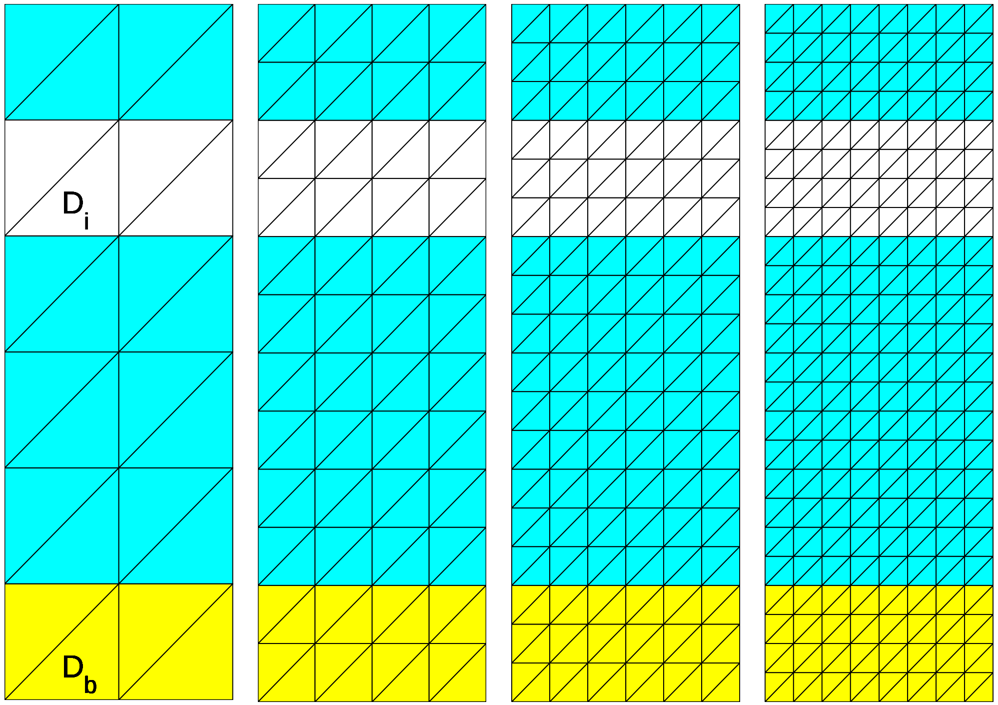

Figure 1: Uniform meshes, with $N = 2, 4, 6, 8$; Interior domain D_i; Boundary region D_b.

Simply supported boundary — Deflection

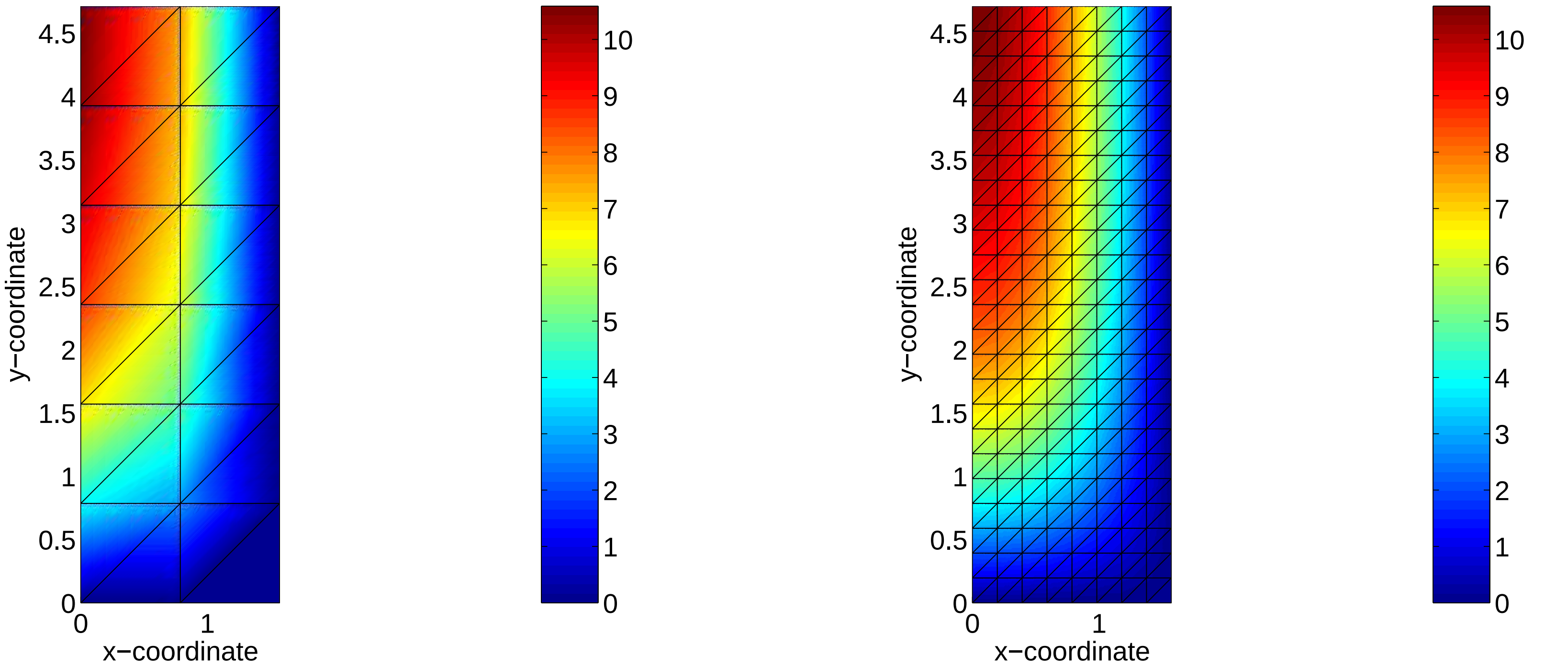

Figure 2: Uniform mesh; Deflection in the discretized domain, with $N = 2, 8$ and $k = 2$.

Simply supported — H^1- and L^2-errors
Interior domain

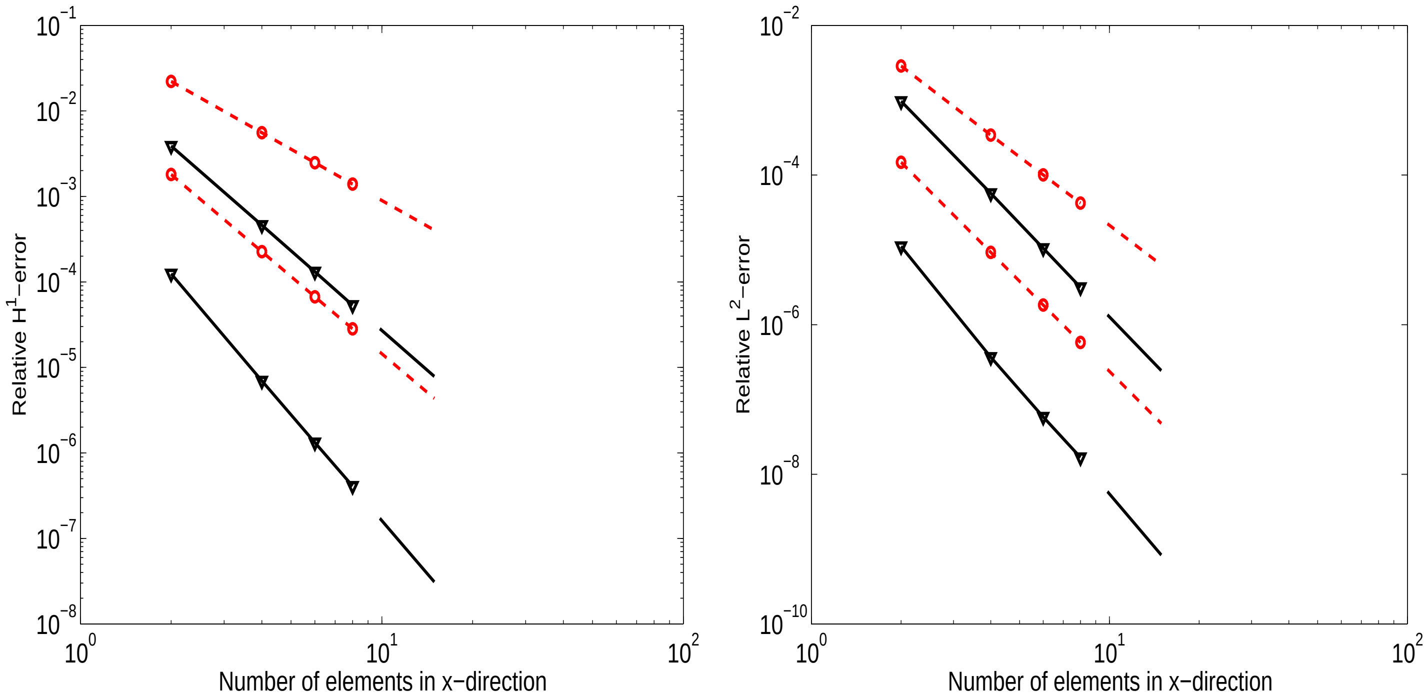

Figure 3: Uniform mesh; Convergence in the H^1- and L^2-norms, with $k = 2, 3$ (**red dashed** line for the **original**, **black solid** line for the **postprocessed** deflection).

Free boundary — Deflection

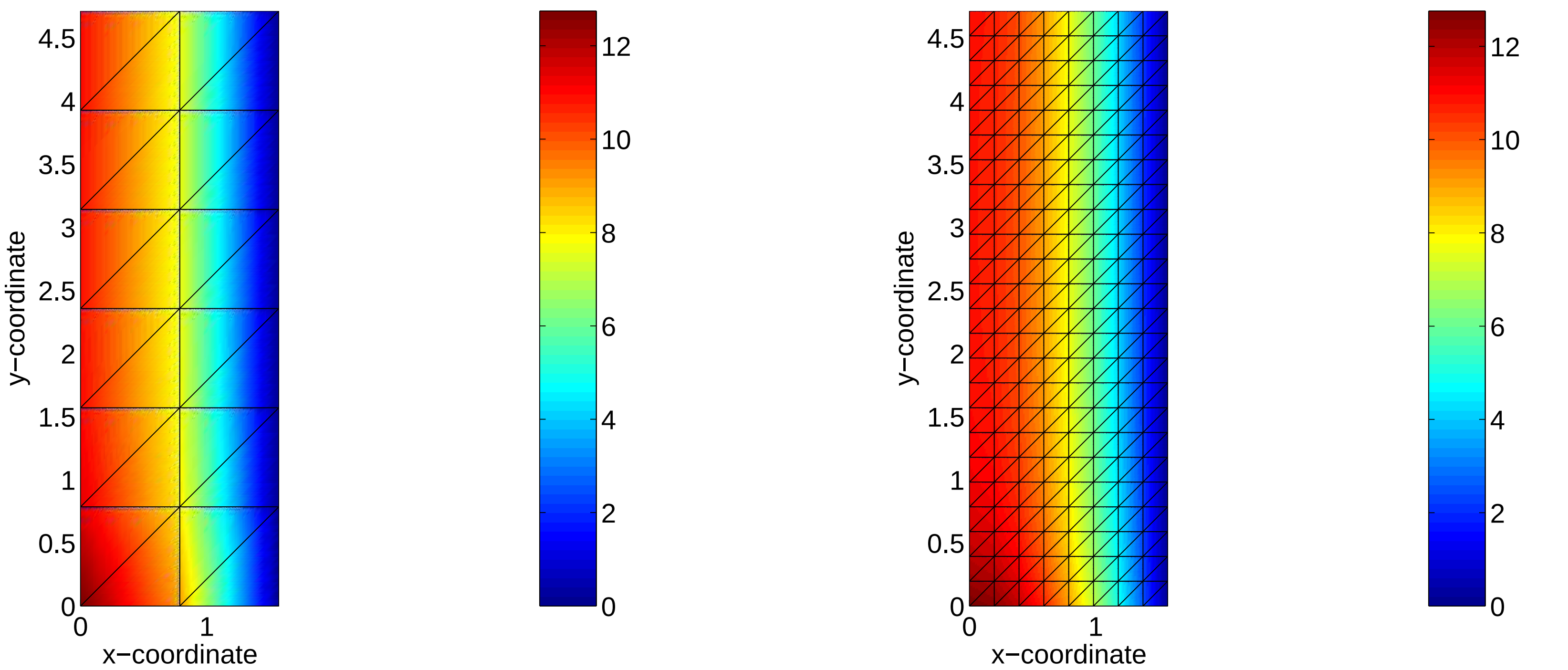

Figure 4: Uniform mesh; Deflection in the discretized domain, with $N = 2, 8$ and $k = 2$.

Free — H^1- and L^2-errors
Interior domain

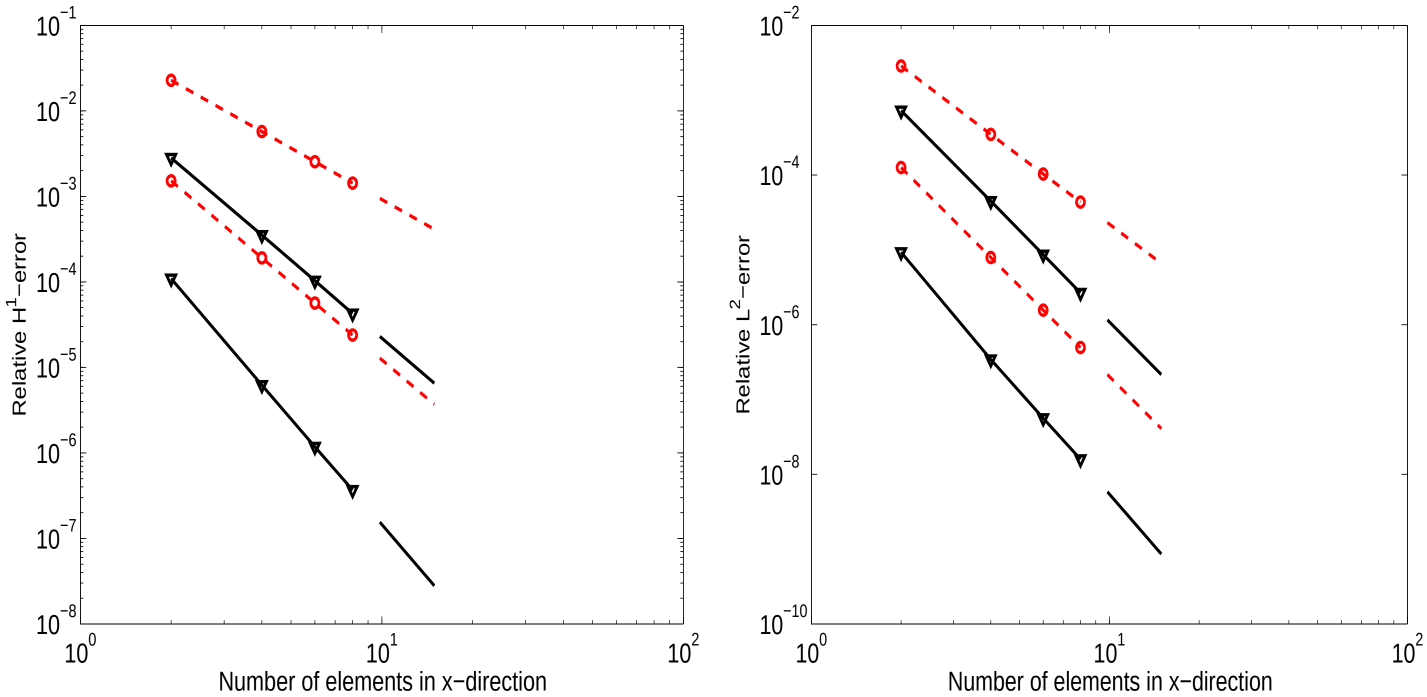

Figure 5: Uniform mesh; Convergence in the H^1- and L^2-norms, with $k = 2, 3$ (**red dashed** line for the **original**, **black solid** line for the **postprocessed** deflection).

Accuracy for the uniform meshes — Boundary region

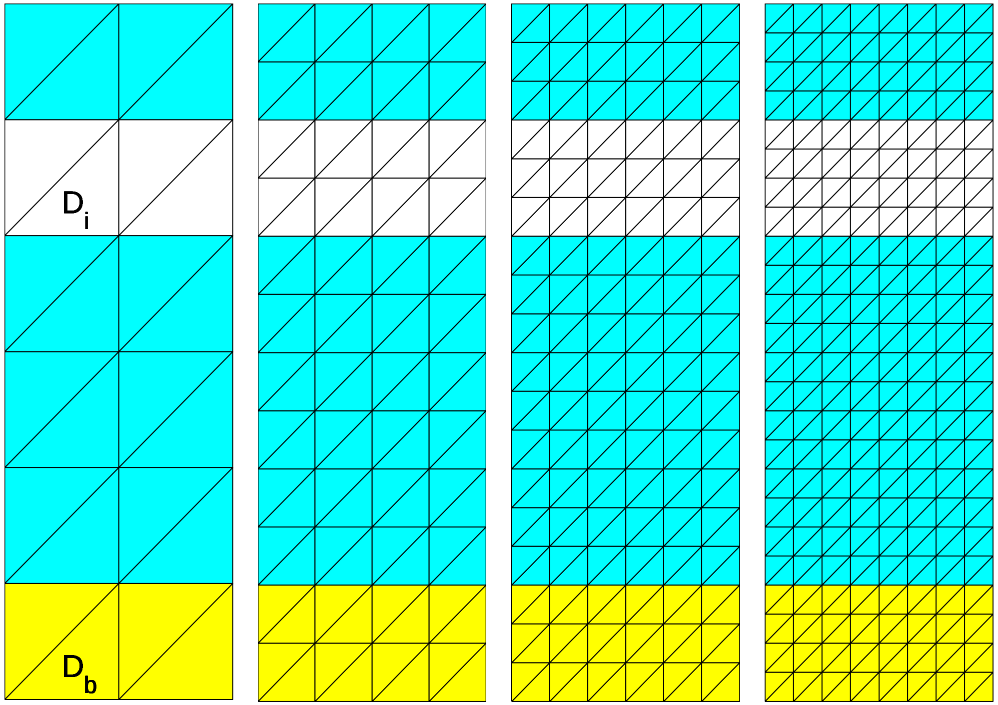

Figure 6: Uniform meshes, with $N = 2, 4, 6, 8$; Interior domain D_i; Boundary region D_b.

Simply supported — H^1- and L^2-errors
Boundary region

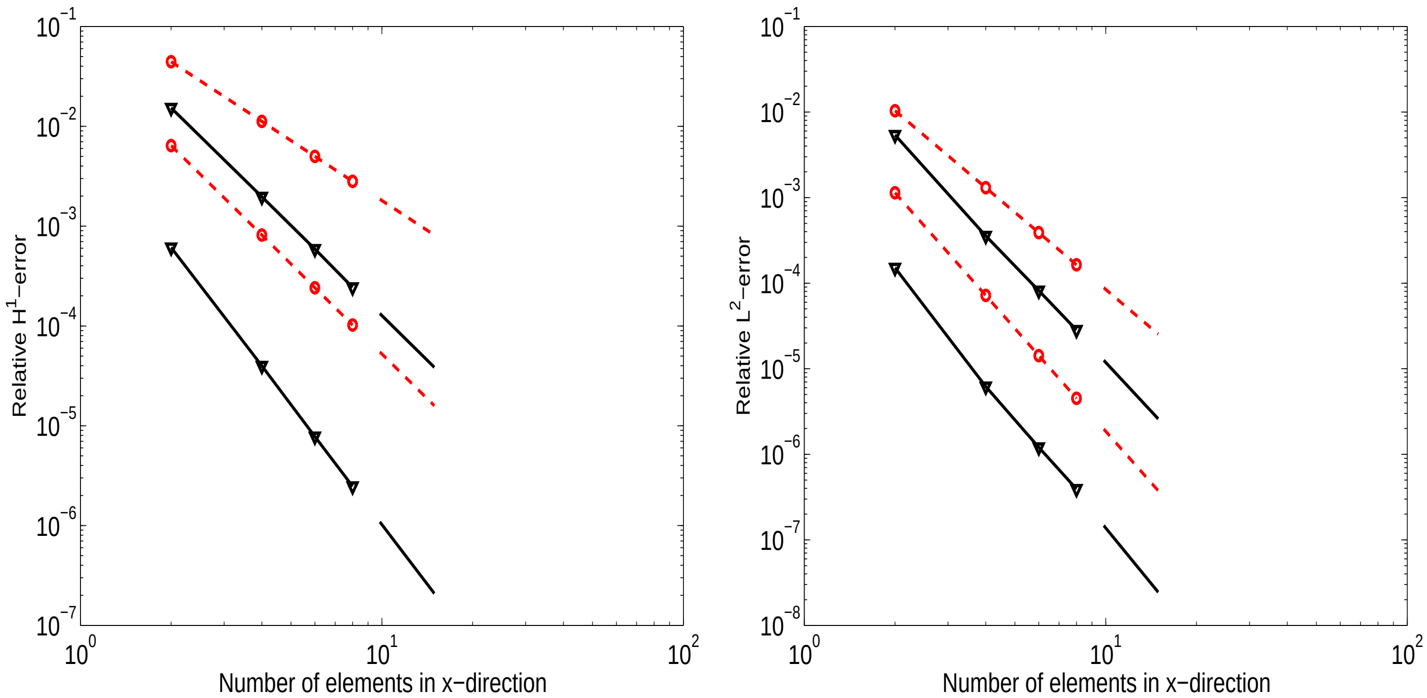

Figure 7: Uniform mesh; Convergence in the H^1- and L^2-norms, with $k = 2, 3$ (**red dashed** line for the **original**, **black solid** line for the **postprocessed** deflection).

Free — H^1- and L^2-errors

Boundary region

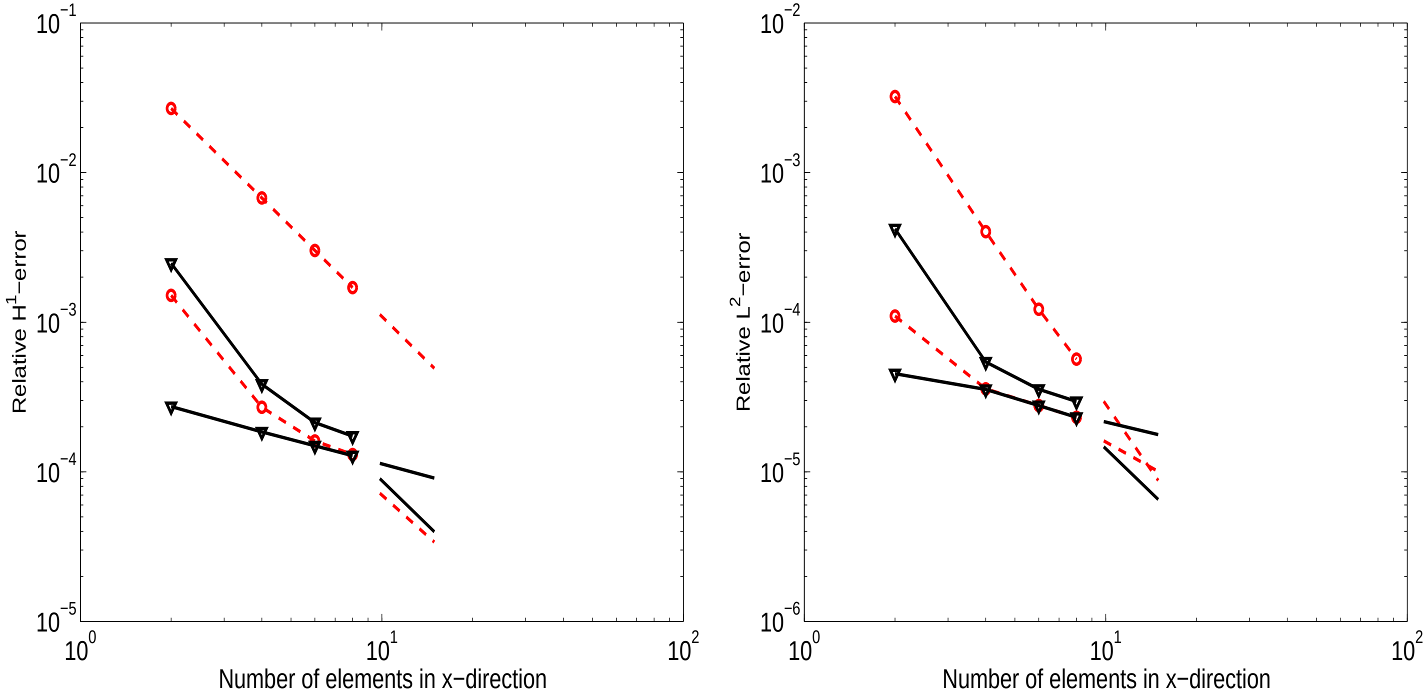

Figure 8: Uniform mesh; Convergence in the H^1- and L^2-norms, with $k = 2, 3$ (**red dashed** line for the **original**, **black solid** line for the **postprocessed** deflection).

Free — Pointwise errors — Along the line $x = \pi/4$

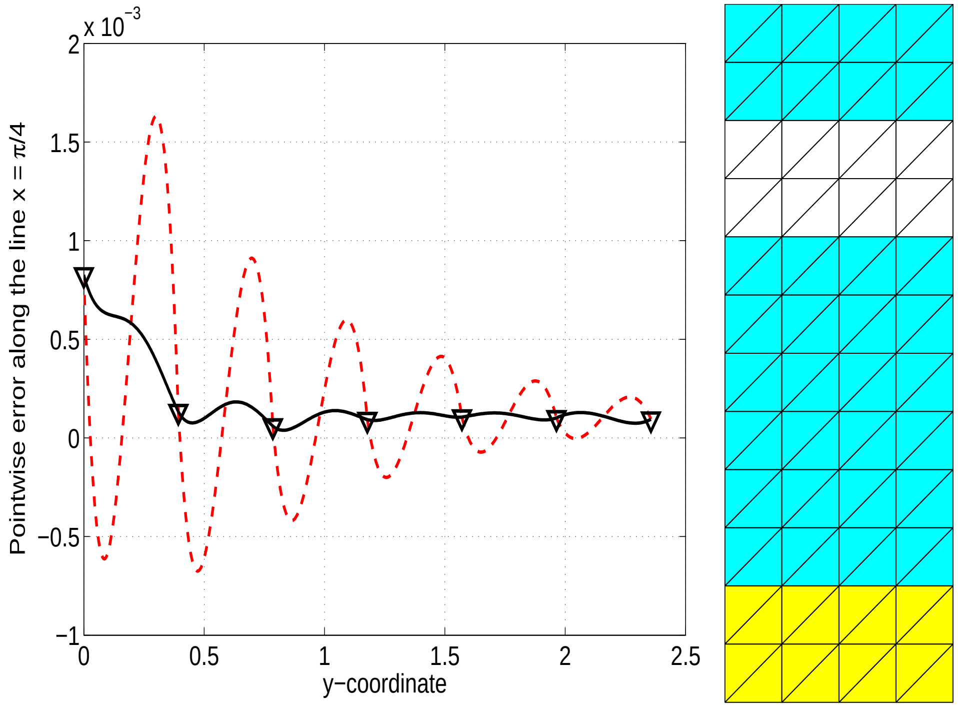

Figure 9: Uniform mesh; Pointwise error on the line $x = \pi/4$, with $N = 4$, $k = 2$ (**red dashed** line for the **original**, **black solid** line for the **postprocessed** deflection, ***triangles*** for the ***vertex values***).

Accuracy for the non-uniform meshes — Boundary region

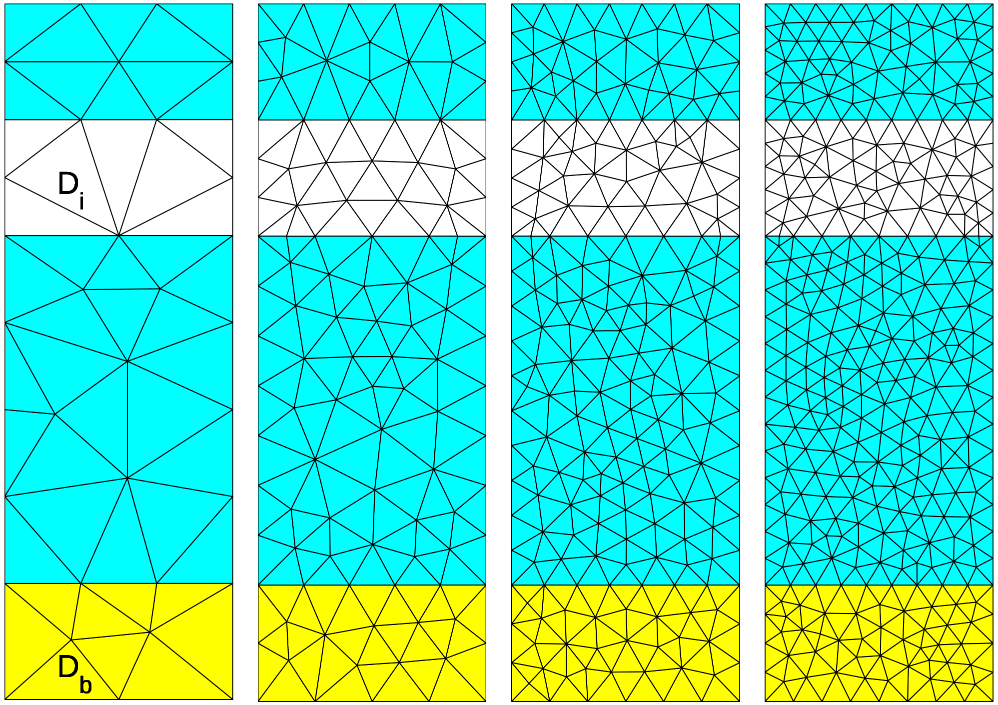

Figure 10: Non-uniform meshes, with $N = 2, 4, 6, 8$; Interior domain D_i; Boundary region D_b.

Simply supported boundary — Deflection

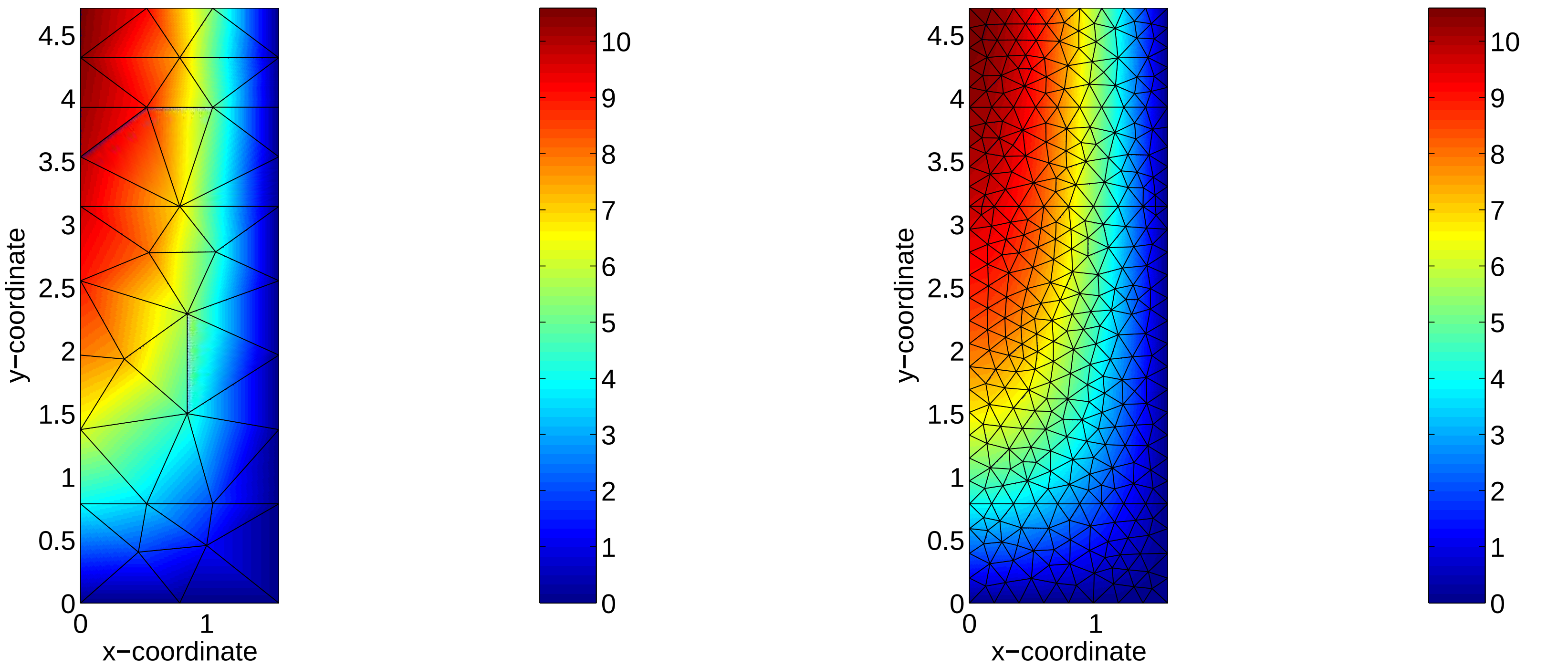

Figure 11: Non-uniform mesh; Deflection in the discretized domain, with $N = 2, 8$ and $k = 2$.

Simply supported — H^1- and L^2-errors
Boundary region

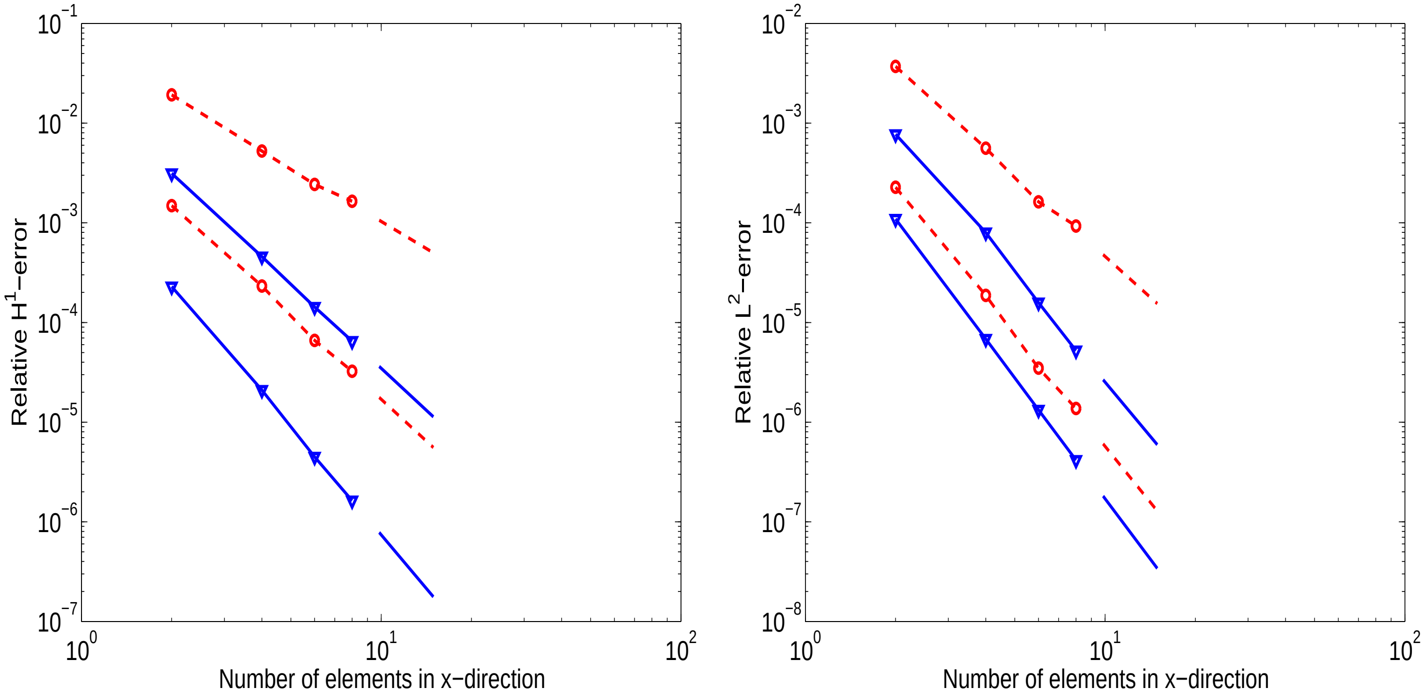

Figure 12: Non-uniform mesh; Convergence in the H^1- and L^2-norms, with $k = 2, 3$ (**red dashed** line for the **original**, **blue solid** line for the **postprocessed** deflection).

Free boundary — Deflection

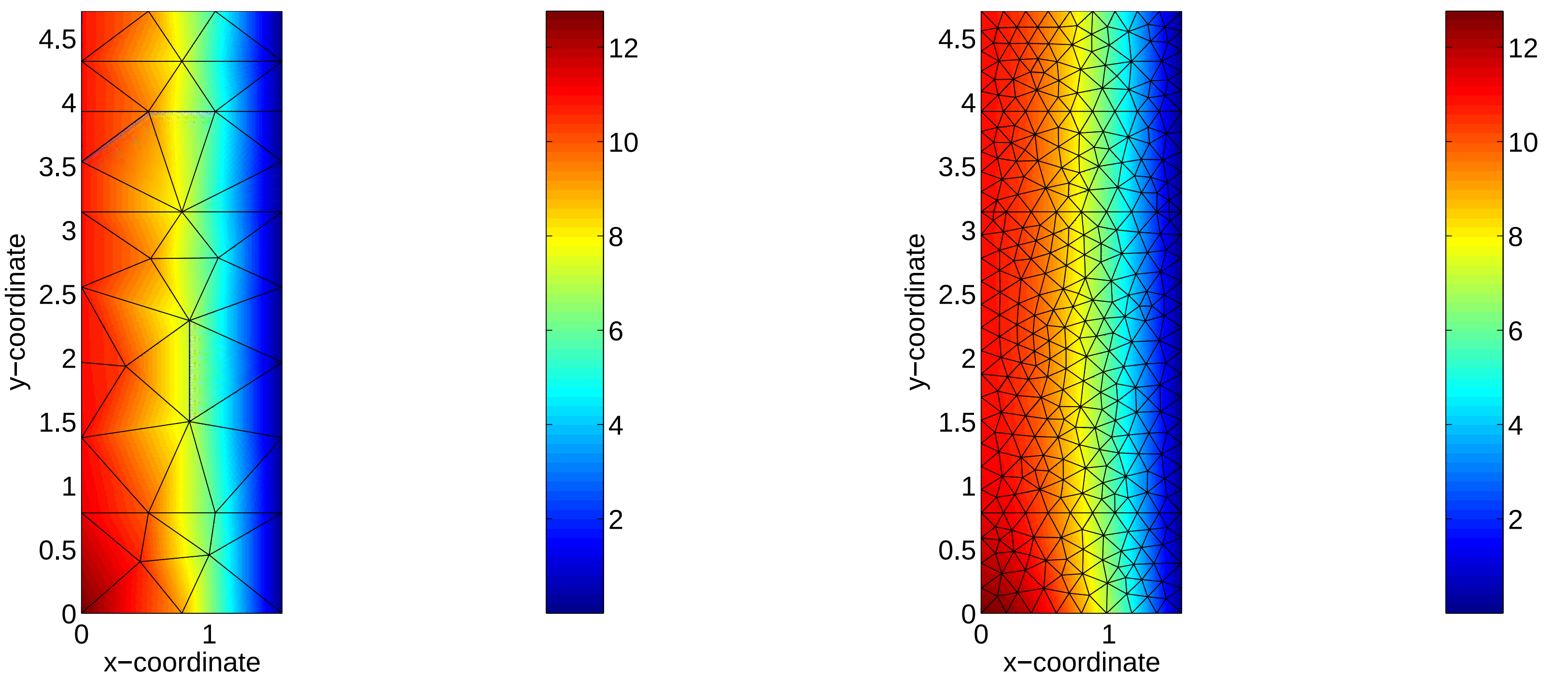

Figure 13: Non-uniform mesh; Deflection in the discretized domain, with $N = 2, 8$ and $k = 2$.

Free — H^1- and L^2-errors
Boundary region

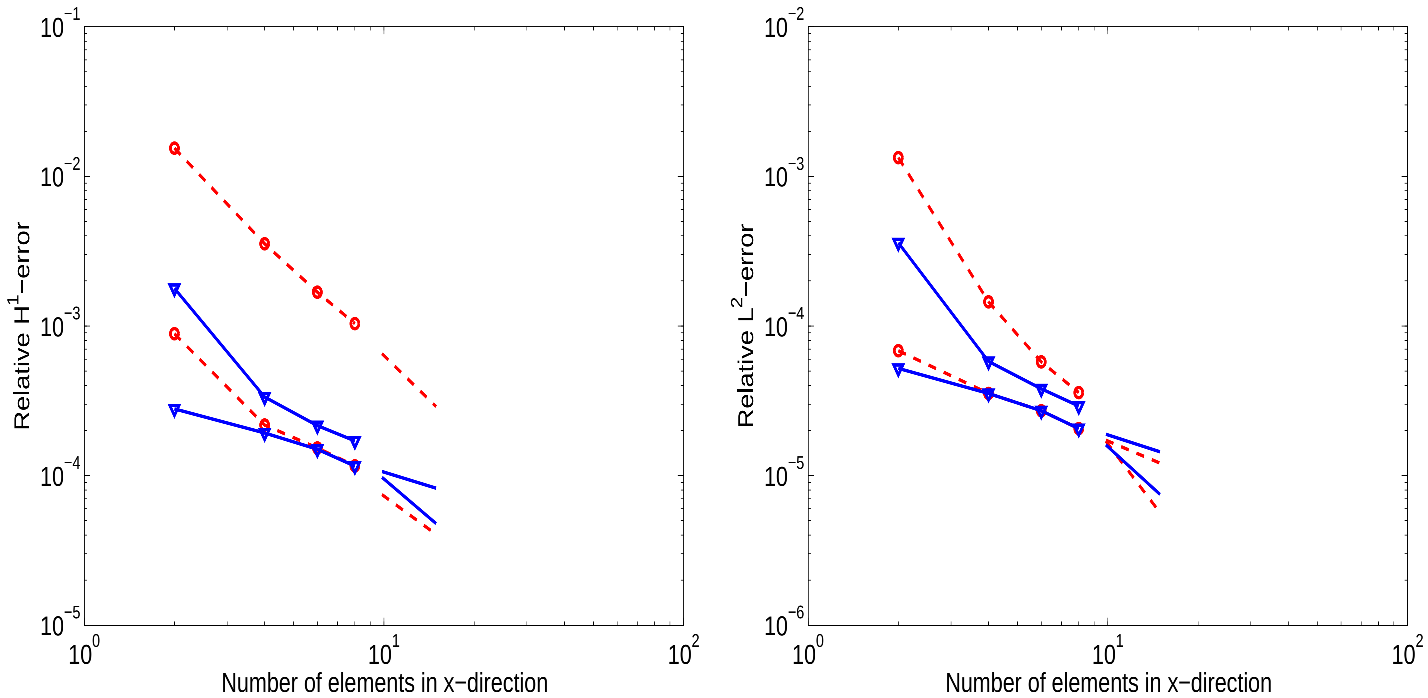

Figure 14: Non-uniform mesh; Convergence in the H^1- and L^2-norms, with $k = 2, 3$ (**red dashed** line for the **original**, **blue solid** line for the **postprocessed** deflection).

Free — Pointwise errors — Along the line $y = \pi/4$

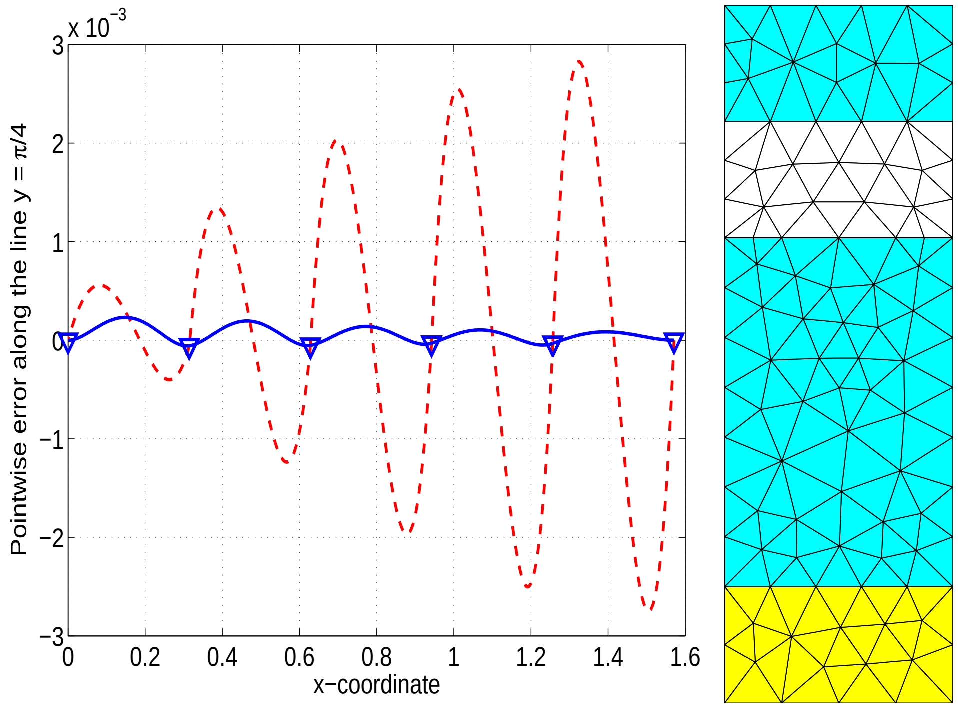

Figure 15: Non-uniform mesh; Pointwise error on the line $y = \pi/4$, with $N = 4$, $k = 2$ (**red dashed** line for the **original**, **blue solid** line for the **postprocessed** deflection, ***triangles*** for the ***vertex values***).

Conclusions

- A superconvergence result in the H^1-norm holds for the original deflection approximation.
- Improved accuracy in the H^1-norm holds for the postprocessed deflection approximation.
- The numerical computations confirm the results, for both uniform and nonuniform meshes.
- Furthermore, the numerical computations
  — indicate similar results also in the L^2-norm and
  — show the superaccuracy of the vertex values.